ADVANCED OPTICAL MATERIALS
www.advopticalmat.de

Interplay of Circularly Polarized Light with Molecular and Structural Chirality: Chiral Lanthanide Complexes and Cellulose Nanocrystals

*Matteo Cei, Alessandra Operamolla, and Francesco Zinna**

The interaction of circularly polarized (CP) light with chiral matter at different scales opens several possibilities of light manipulation in photonic and electronic devices. Here it is shown that in a multilayer architecture, it is possible to take advantage of the polarization-selective reflection of the nematic arrangement of cellulose nanocrystals and the strong intrinsic CP luminescence (CPL) of the various bands of chiral Eu complexes. In this way, both the intrinsic CPL and total emission of the complex are modified depending on the enantiomer applied and on the detection geometry. This concept may apply for polarization control in electronic and photonic devices and polarized optical cavities.

1. Introduction

The generation of circularly polarized (CP) light and its interaction with chiral matter is a topic of relevant interest with multifarious applications[1] in chiral photonics and electronics,[2–9] advanced and smart materials,[10] etc.

Chirality can be observed at multiple scales, from molecules to meso or macro supramolecular structure, giving rise to different properties.[11,12] At each hierarchical scale CP light can interact with matter through different physical mechanisms.[13–15] This is a relevant topic in photonic materials and devices. Indeed, the interplay between CP light and chirality from molecules to mesoscopic structures has implications in the engineering of electronic devices, such as CP-OLEDs and CP-detectors,[16–19] chiral resonant and lasing cavities,[20–22] etc. In all these cases, it is fundamental to understand and manipulate the outcoupling of light polarization and to harness the effects on emitted or absorbed CP light of chiral elements and structures at various scales.

Mesoscale systems displaying helical structures with a pitch of the same order of visible or near infrared wavelengths are employed to control CP light in a passive way through their reflection bands. Examples of photonic materials able to control the CP light in such a way are chiral nematic liquid crystals (CNLC).[23–25] These systems display a selective reflection band showing the circular Bragg phenomenon, i.e., a preferential reflection of CP light with a certain handedness and the subsequent transmission of the opposite one. For normal light incidence, the wavelength position (λ) of the reflection band depends on the average refractive index (n_{avg}) and the helical pitch P:

$$\lambda = n_{avg}\, P \tag{1}$$

If the reflection wavelength is comprised between $n_oP < \lambda < n_eP$, with n_o and n_e being the ordinary and extraordinary refractive indices respectively, the variation of the dielectric tensor within the material describes a helix. In this regime, the reflection is selective for the CP component matching the handedness of the helical structures forming the chiral nematic phase.[26]

An interesting example of a natural photonic material forming CNLC phases upon film deposition is given by cellulose nanocrystals (CNC).[27–29] CNCs are defined as short stick-shaped crystalline nanoparticles with a diameter ranging from 5 to 50 nm and a length between 100 and 500 nm, according to TAPPI (*Technical Association of Pulp and Paper Industry*) standards.[30] CNCs, being composed of cellulose, the structural biopolymer derived from plants, are affordable and environmentally friendly nanomaterials useful for many applications in the field of materials and biomedical science.[31–35] CNCs prepared under sulfuric acid hydrolysis are negatively charged as a consequence of their surface sulfation.[36] Sulfated CNCs can self-organize in the solid state to minimize the electrostatic surface repulsion. They demonstrate chiral nematic lyotropic liquid crystal phase formation, which tends to be retained after evaporation of the water solvent.[37] Films containing domains with oriented crystals[38,39] macroscopically result in a brilliantly colored iridescence arising from the solid-state films prepared under specific slow-evaporation conditions.[38–41] Moreover, CNCs show a

M. Cei, A. Operamolla, F. Zinna
Dipartimento di Chimica e Chimica Industriale
University of Pisa
Via Moruzzi 13, Pisa I-56124, Italy
E-mail: francesco.zinna@unipi.it
M. Cei, A. Operamolla
Interuniversity Consortium of Chemical Reactivity and Catalysis (CIRCC)
Via Celso Ulpiani, 27, BariI-70126, Italy

The ORCID identification number(s) for the author(s) of this article can be found under https://doi.org/10.1002/adom.202401714

DOI: 10.1002/adom.202401714

selective reflection of left CP light, with the distinctive advantage of a wide tunability of their reflection band. The reflected wavelength can be controlled by using additives such as NaCl, glucose, or glycerol, or by physical methods,[41–45] spanning from the near-infrared to the UV region. These properties, beyond CP light production,[46–48] are exploited for CP detection,[49] in anticounterfeiting photonic tags,[50] chiral cavities,[51] cancer cell discrimination in tissues,[52,53] etc.

At the opposite end of the dimensional scale, isolated (i.e., non-aggregated) chiral emitting molecules generate CP luminescence (CPL) thanks to a coupling between their intrinsic electric (μ_{ij}) and magnetic (m_{ij}) transition dipole moment.[54] In these systems, the dissymmetry factor g_{lum} depends on m and μ according to:

$$g_{lum} = 4\frac{\boldsymbol{m}_{ij} \cdot \boldsymbol{\mu}_{ji}}{\left|\boldsymbol{\mu}_{ji}\right|^2 + \left|\boldsymbol{m}_{ij}\right|^2} \quad (2)$$

Most molecular compounds show CPL activity with dissymmetry factors within the order of 10^{-4}–10^{-2} and overall modest CPL brightness factors.[55,56] On the other hand, intriguing properties are showcased by lanthanides, and in particular Eu(III)'s chiral complexes, which may show exceptionally high g_{lum} factors, often with strong CPL brightness, associated to their *f*–*f* transitions in the orange/red region.[4,56–65] They also usually show bands, associated to intraconfigurational transitions among different *J* levels, with opposite polarizations.

These two very different mechanisms of CP light generation/discrimination (one produced at the mesoscale by CNCs' ordered self-aggregation, the other through emission from enantiopure lanthanide chiral complexes) could in principle synergically operate. In particular, their simultaneous presence could significantly modify the intrinsic CPL and total emission spectrum of the chiral emitter. So far, the generation of CPL by using CNCs and optically inactive emitters has been reported in various instances in the literature,[66–71] but the interplay between the intrinsic polarization of chiral emitters with the structural polarization properties of CNC films in various configurations has been rather overlooked. To observe a significant mesoscale-induced modification of the molecular CPL, it is critical that the polarization contribution of the CNC and the intrinsic CPL activity of the chiral-emitting materials are of a similar magnitude. As mentioned above, such performances are usually not given by purely organic emitters or most *d*-metal coordination compounds.

Here we show that the deposition of suitable chiral lanthanide complexes on a CNC layer with a tuned reflection band generates amplification/attenuation effects on the different CPL transitions of chiral Eu complexes. Moreover, the mesoscale-induced modification of the molecular CPL results in significant differences of the total emission spectrum of Eu(III) enantiomeric complexes. This is made possible thanks to Eu transitions featuring opposite polarization, which is again a characteristic of lanthanide complexes.

2. Results and Discussion

Cellulose nanocrystals were prepared by sulfuric acid hydrolysis from Whatman paper. The field emission scanning electron microscopy (FE-SEM) micrograph (inset of **Figure 1a**; Figure S1, Supporting Information) showed nanorod morphology with an average length below 100 nm. The CNC iridescent films were prepared by solution casting from a 3% (w/w) suspension of S-CNCs that was allowed to evaporate at room temperature to yield self-standing films with a thickness of ≈110 µm (standard deviation SD = 10 µm). Such thickness provides a good trade-off between the polarization properties (see below) and a sufficient transmittance (T) of the film (T ≈ 20%). The cross-section of the freestanding films was analyzed by FE-SEM, showing the cholesteric nematic ordering of the as-cast thin films (Figure 1a). It is noted that due to the soft nature of the CNC films, some artifacts may occur due to the burning of the fracture surface under the electron beam. These artifacts may produce local collapse of layers or misalignment of protruding CNCs.[72]

The films showed a photonic band gap ≈850 nm, with an associated strong circular extinction measured as differential optical density ($\Delta OD = OD_L - OD_R$, $OD_{L/R}$ being the optical densities for left/right CP light). The maximum of the band could be blue-shifted down to 450 nm by addition of weight percentages of NaCl (Figure S2, Supporting Information). The conditions were optimized to shift the reflectance band ≈600 nm to match Eu emission (Figure 1c). The as-cast films were characterized through circular dichroism, to measure the differential optical density. As expected, we observed a strong positive circular extinction ($\Delta OD \approx 0.30$, $\Delta OD/OD \approx 0.52$, SD = 0.09) due to the selective reflection of left-handed CP light (Figure 1b). Having established the methodology to prepare iridescent films with the desired reflectance band, we proceeded to prepare multi-layered films by means of depositions from orthogonal solvents. A toluene solution of PMMA and the desired emissive Eu(III) complex was deposited by spin-coating on a dry CNCs film (Figure 1d). The Eu/PMMA layer is completely transparent in the visible, and its deposition does not affect the position and circular extinction of the photonic band of the CNC (Figure S3, Supporting Information).

All the films show the expected Eu(III) emission in the red region with sharp bands stemming from the $^5D_0 \rightarrow {}^7F_J$ transitions under 365 nm irradiation (Figure 1e,f). The discussion will be focused on the magnetically allowed transition $^5D_0 \rightarrow {}^7F_1$ (595 nm), where the highest g_{lum} factors are often observed, and the hypersensitive one $^5D_0 \rightarrow {}^7F_2$ (610–620 nm), giving the most intense emission band.

The emergent CPL of the multi-layered films can be measured in two different configurations depending on the orientation of the film with respect to the detector, as shown in Figure 1g,h. The CPL measurement can be carried out with i) the emissive layer behind the CNC film, with respect to the detector (E-CNC-D, i.e., transmission mode, Figure 1g); ii) the emissive layer between the CNC film and the detector (CNC-E-D, reflection mode, Figure 1h). The role of the CNC in the two configurations is radically different (see below). In both configurations, we can calculate the emergent CPL dissymmetry factor of the multilayer films $\tilde{g}$ following the usual definition:

$$\tilde{g} = 2\frac{I_L - I_R}{I_L + I_R} \quad (3)$$

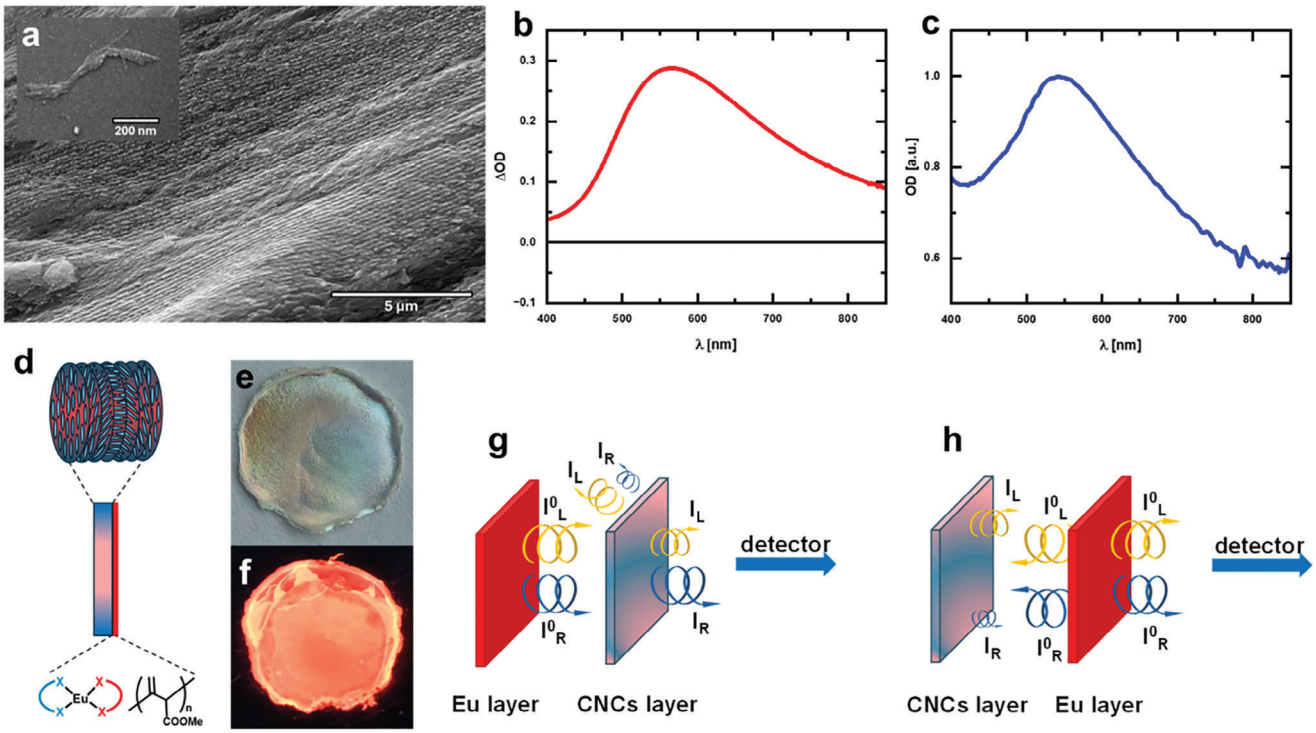

Figure 1. a) FE-SEM micrograph of the cross-section of a free-standing CNC film. Scale bar 5 µm. Inset: FE-SEM micrograph of CNCs aggregate deposited on glass from a 1 mg L^{-1} water dispersion. Scale bar: 200 nm. Circular b) and total extinction c). d) Structure of the multilayer films with images under daylight e) and 365 nm light f). g,h) Effects of the measurement configurations on the circular polarization of light.

With I_L and I_R being the left and right polarized components of the emerging emission.

We started with an optically inactive complex: $Eu(TTA)_3Phen$ (TTA = thenoyltrifluoroacetone, Phen = 1,10-phehanthroline, **Figure 2a**), which is characterized by a strong luminescence (Figure S4, Supporting Information), but null intrinsic CPL activity. The CPL spectrum obtained with the film in the E-CNC-D configuration shows a negative sign throughout the whole measured range with an emergent constant $\tilde{g}$ value of −0.18. These values are in agreement with what observed with optically inactive Eu complexes dispersed in CNC films.[69] On the other hand, positive CPL signals ($\tilde{g}$ =0.19) are observed in the CNC-E-D configuration (Figure 2b; Table S1, Supporting Information). In the first case, the CNCs film acts as a filter, reflecting some of the left polarized light away from the detector and transmitting mainly the right CP light, therefore $I_L - I_R < 0$. In the second case, the light emitted directly toward the detector is not polarized and does not contribute to the CPL signal, while part of the light

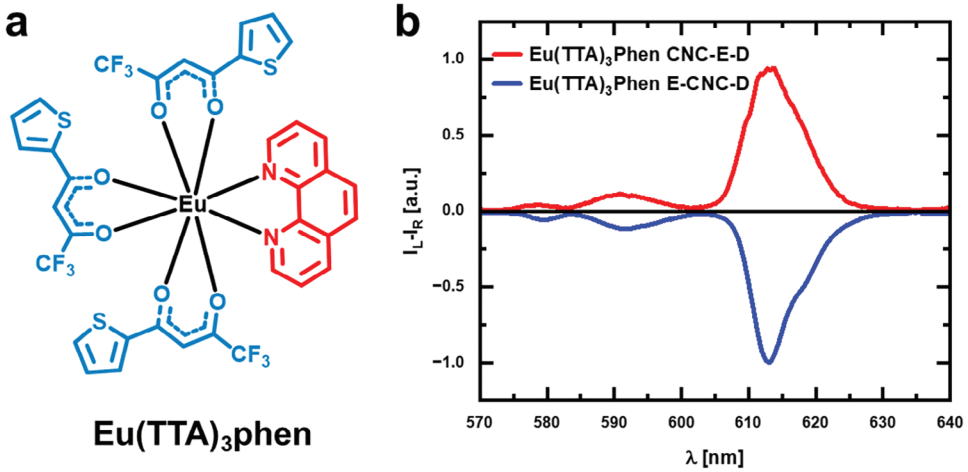

Figure 2. a) Structure of optically inactive $Eu(TTA)_3Phen$; b) normalized CPL spectrum of the multilayered film containing $Eu(TTA)_3Phen$ measured in CN-E-D and E-CNC-D configuration.

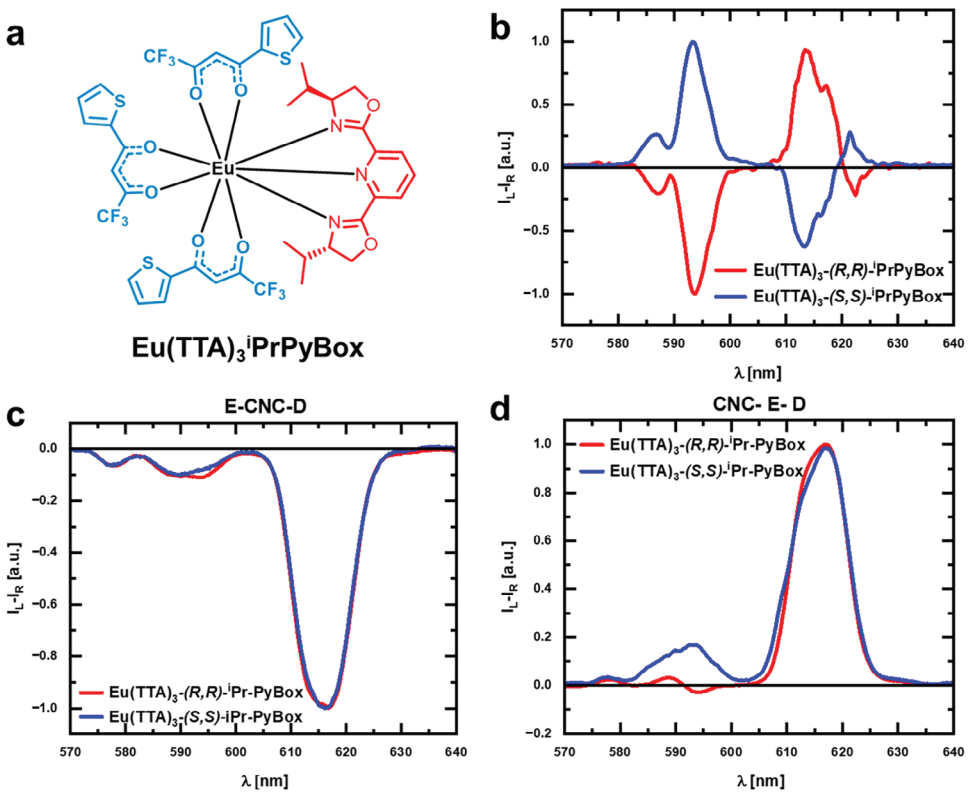

Figure 3. a) Structure of Eu(TTA)$_3$[i]PrPyBox; b) normalized CPL spectrum of the two enantiomers of Eu(TTA)$_3$[i]PrPyBox in PMMA film; normalized CPL spectra of the multilayered films containing the two enantiomers of the complex in E-CNC-D c), and CNC-E-D d) configuration.

emitted backward, toward the CNCs film, is reflected back to the detector. This portion of light, being mainly left polarized, gives a positive CPL signal.

Having demonstrated the polarizing capabilities of the prepared CNCs films, we increased the complexity of the multi-layered systems by using an enantiomer pair of an optically active europium complex. For this purpose, enantiomeric Eu(TTA)$_3$[i]PrPyBox ([i]PrPyBox = 2,2′-(2,6-pyridinediyl)bis(4-isopropyl-2-oxazoline) complexes, **Figures** 3a, and S5, Supporting Information) were chosen, due to its high dissymmetry factor and overall CPL brightness.[5,73] The intrinsic CPL spectra of the (R,R) and (S,S) enantiomers of this species in PMMA films are characterized by two main bands with opposite sign and different dissymmetry factors ($|g_{lum}|$ 0.02 at 614 nm and 0.2 at 595 nm, according to Equation 3, Figure 3b).

As in the previous case, the CPL spectra of the bi-layered films are measured both in the transmission (E-CNC-D) and in the reflection (CNC-E-D) configurations. With an optically active complex, the CPL of the composite films is expected to be the result of the convolution of the intrinsic polarization of the luminescence from the molecular complex, and the circular Bragg phenomenon associated with the structural chirality of the CNCs layer. As seen in the case of the optically inactive Eu(TTA)$_3$Phen, the contribution from the CNC layer to the polarization maintains the same sign throughout the whole spectral range investigated. This ensures different effects on the two bands of the optically active Eu complex. When the intrinsic Eu CP contribution is concordant with the polarization dictated by the CNC, the total signal is expected to have a higher intensity compared to the corresponding signal in the spectrum of the complex. Conversely, when the complex CPL and CNC effects operate in an opposite way, the resulting CPL band is expected to be reduced in intensity.

The spectra of both the Eu(TTA)$_3$-*(R,R)*-[i]PrPyBox/CNCs and the Eu(TTA)$_3$-*(S,S)*-[i]PrPyBox/CNCs films, acquired in the E-CNC-D configuration, exhibit a negative peak for the $^5D_0 \rightarrow {}^7F_2$ transition at 614 nm. Such band, being of induced electric dipole character, has a weak intrinsic g_{lum} (0.02), therefore its emergent polarization is dominated by the negative CNC contribution ($\Delta OD/OD \approx 0.52$). Therefore, a complete inversion for the signal of the *(R,R)* enantiomer is observed. In the E-CNC-D configuration, the $\tilde{g}$ factor observed for this band is −0.17 in line with the one observed for Eu(TTA)$_3$Phen. On the other hand, the magnetic dipole transition at 595 nm appears slightly reduced in the case of *(S,S)* enantiomer compared to *(R,R)* one ($\tilde{g}$ −0.15 vs −0.17, Figure 3c). Even more noticeable, in the CNC-E-D configuration, the 595 nm band of the *(R,R)* enantiomer is almost canceled ($\tilde{g} = -0.01$) by the opposite effects of the intrinsic polarization of the complex with respect to the selective reflection of the CNC film (Figure 3d; Table S1, Supporting Information)

To demonstrate the generality of this approach, we prepared different multi-layered films using a different europium complex. CsEu(hfbc)$_4$ (hfbc = heptafluorobutyryl camphorate, **Figure** 4a; Figure S6, Supporting Information) was chosen as it displays the highest g_{lum}, associated to the 595 nm band, reported to date for any lanthanide complexes.[16,74–77] The quantum yield of this complex is lower than that of Eu(TTA)$_3$[i]PrPyBox, but its

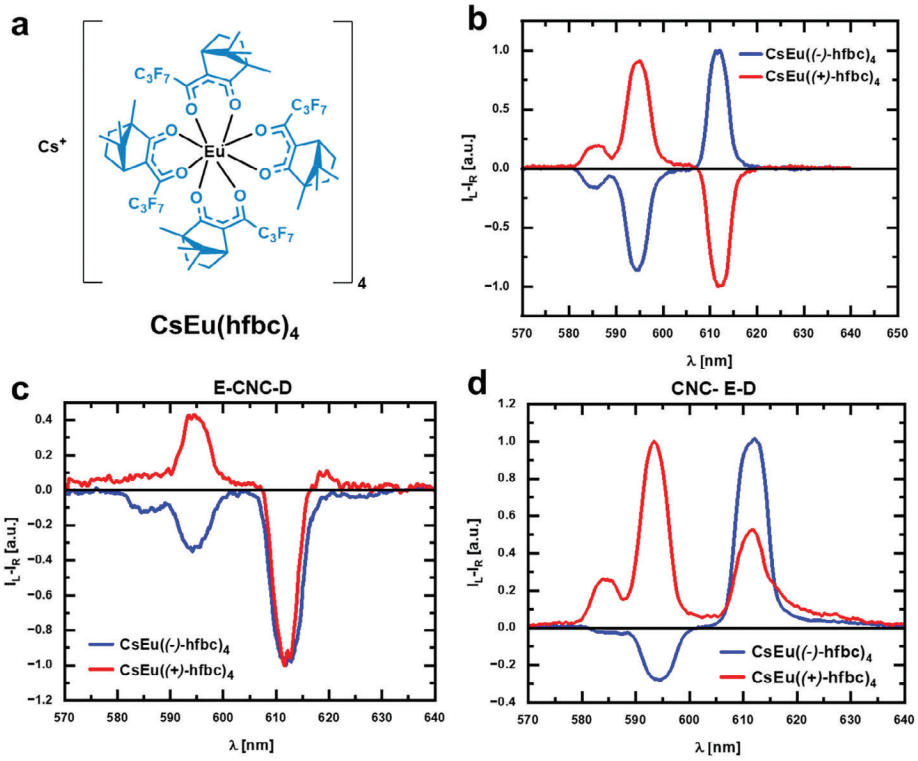

Figure 4. a) Structure of CsEu(hfbc)$_4$; b) normalized CPL spectrum of the two enantiomers of CsEu(hfbc)$_4$ in PMMA film; normalized CPL spectra of the multilayered films containing the two enantiomers of the complex in E-CNC-D c), and CNC-E-D d) configuration.

high dissymmetry factors assure a high CPL brightness. PMMA films containing 2% of CsEu(hfbc)$_4$, showed $|g_{lum}|$ of 1.38 and 0.23 for the transition at 595 and 614 nm, respectively (Figure 4b). The association of the complex with the CNC film strongly modifies its intrinsic polarization. In the E-CNC-D configuration, the peak at 614 nm is negative for both the enantiomers of the complex, as the CNC selective reflection determines the final polarization. On the other hand, for the 595 nm band, the higher intrinsic polarization of the complex dominates over the CNC extrinsic contribution (Figure 4c). A similar but opposite trend is observed for the CNC-E-D configuration (Figure 4d). Due to the strong intrinsic polarization of the 614 nm band in the case of the CsEu(hfbc)$_4$ complexes, this contribution undergoes dramatic changes, as its emergent polarization is no longer controlled by the CNC selective reflection alone. This is especially evident in the CNC-E-D configuration, where the relative sign and intensity of the CPL bands associated to the 595 and 612 nm transitions change dramatically in multilayer films containing the two enantiomers of the complex (see also Table S1, Supporting Information).

We took care to rule out potential interference from linear contributions in the measured spectra by measuring linear diattenuation and luminescence linear anisotropy. In all cases, the measured linear contributions are negligible with respect to the genuine CP signals (Figures S12–S14, Supporting Information).

In the case of the E-CNC-D configuration, the emergent CPL spectral profile ($\widetilde{CPL}$) of the multilayered films can be modeled by treating the emission of the photons from the complex and their interaction with the CNC film as independent events. We have to consider (i) the differential optical density (ΔOD) of the CNC layer at each wavelength, which accounts for the circular Bragg phenomenon; (ii) the g_{lum}-versus-wavelength plot of the CPL of the complex in the PMMA film and its emission spectrum I(λ), (see the SI for the derivation):

$$\widetilde{CPL}(\lambda) = 2\frac{1-\gamma\cdot 10^{\Delta OD}}{1+\gamma\cdot 10^{\Delta OD}}\cdot I(\lambda) \quad (4)$$

with

$$\gamma = \frac{2-g_{lum}}{2+g_{lum}} \quad (5)$$

Despite the simplicity of the model, Equation 4 is able to qualitatively reproduce the CPL spectral features observed for the multilayered films (Figure S10, Supporting Information). On the other hand, the model neglects other possible contributions to the emergent CPL, such as depolarization effects within the multilayer film or interface effects between the PMMA/complex and the CNC layer.

Last, we investigated the effects of the interplay between the polarized emission of CsEu(hfbc)$_4$ and CNC layer on the total emission spectra for the multi-layered films. As part of the left CP light emitted by the complex is not transmitted by the selective reflection of the CNC film, a different effect on the various emission bands of the complex is predictable, potentially modifying the total emission spectral profile. Given the high intrinsic polarization of the magnetically allowed transition of CsEu(hfbc)$_4$

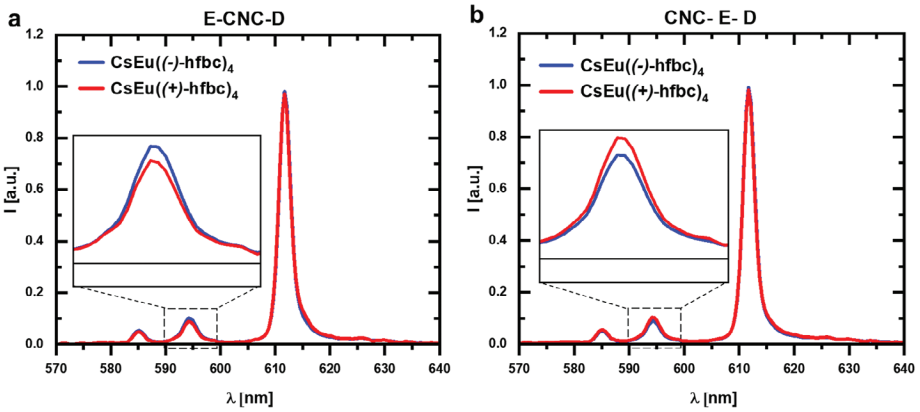

Figure 5. Total emission of multilayer films containing the two enantiomers of $CsEu(hfbc)_4$ in E-CNC-D a) and CNC-E-D b) configuration. The insets show a zoom-in of the 595 nm band.

(595 nm), a differential attenuation of the total luminescence of this band for the two enantiomers is expected, while a much smaller effect is predicted for the 614 nm one. In the case of $CsEu((+)\text{-}hfbc)_4 \approx 80\%$ of the emitted photons associated to the 595 nm transitions are left-handed polarized, while for the opposite enantiomer, the majority of the photons have the opposite polarization (80% right-handed). Therefore, the preferential reflection of the CNC film toward left-handed CP light will cause a more pronounced effect in the case of (+) enantiomer. This is indeed seen as a more pronounced dimming for the 595 nm band in the case of films containing (+) enantiomer with respect to the (−) one in the E-CNC-D configuration. Note that the polarization effects of the CNC layer are the same in both cases.

Indeed, in the total luminescence, the ratio between the intensity of the 595 nm band and the intensity of the 614 nm band is higher for the $CsEu((-)\text{-}hfbc)_4$/CNCs film compared to the $CsEu((+)\text{-}hfbc)_4$/CNCs one, with the former being 0.1011 (SD = 0.0005) and the latter being 0.088 (SD = 0.004) (**Figure 5a**). On the other hand, in the CNC-E-D configuration, the values are almost inverted, with a ratio of 0.100 (SD = 0.001) for the (+) enantiomer and a ratio of 0.085 (SD = 0.001) for the (−) one (Figure 5b). A plot of the difference between the total luminescence of CNC/$CsEu((+)\text{-}hfbc)_4$ and CNC/$CsEu((-)\text{-}hfbc)_4$ in both E-CNC-D and CNC-E-D configuration is reported in Figure S11 (Supporting Information).

Applying this principle, the presence of CNC would allow for the identification of one enantiomer of the Eu complex over the other, simply by the inspection of the total emission spectrum, without the aid of polarization optics.

Finally, to put in context the performances of the materials presented in this work (see Table S2, Supporting Information), it is useful to consider also their costs. We estimated a cost range of 0.34–0.47 €/film and 0.14–0.28 €/film (a film is approximately 1 cm^2) for CNC films based on $Eu(TTA)_3{}^{i}PrPyBox$ and $CsEu(hfbc)_4$, respectively (see SI).

3. Conclusion

In conclusion, we have shown an interesting interplay between mesoscale and molecular chirality with CP light. The highly polarization-selective reflection band of CNCs can be coupled with the high intrinsic CPL of chiral lanthanide complexes. Eu/CNC multilayer films display very different emergent CPL spectra depending on the enantiomer used and the geometry of detection. Moreover, thanks to the opposite circular polarization associated to the various *f–f* transitions, the presence of CNC modifies the total emission spectrum of the Eu complex depending on the enantiomer used. These principles can be applied in several cases in the design of multilayered materials for polarization control and fine-tuning in devices and polarized optical cavities.

Supporting Information

Supporting Information is available from the Wiley Online Library or from the author.

Acknowledgements

M.C. and A.O. acknowledge CIRCC and Progetto Competitivo 2022 CMPT222955 MUR for funding. The authors acknowledge CISUP (Center for Instrument Sharing of the University of Pisa) for access to the FE-SEM (Dr Randa Anis Ishak) facility. Prof. Silvia Vignolini (Max Planck Institute) and Dr Rosarita D'Orsi (UNIPI) are thanked for useful scientific discussions.

Open access publishing facilitated by Universita degli Studi di Pisa, as part of the Wiley - CRUI-CARE agreement.

Conflict of Interest

The authors declare no conflict of interest.

Data Availability Statement

The data that support the findings of this study are available in the supplementary material of this article.

Keywords

chiral emitters, CNC, CPL, Europium, mesoscale chirality, polarization control

Received: June 28, 2024
Revised: August 20, 2024
Published online:

[1] J. Crassous, M. J. Fuchter, D. E. Freedman, N. A. Kotov, J. Moon, M. C. Beard, S. Feldmann, *Nat. Rev. Mater.* **2023**, *8*, 365.
[2] T. Wang, S. Sun, X. Jiang, X. Ma, *Adv. Opt. Mater.* **2024**, *12*, 2301770.
[3] S. Zhao, G. Li, Q. Guo, Y. Wang, M. Zhang, Y. Zhou, S. Jin, M. Zhu, T. Zhuang, *Adv. Opt. Mater.* **2023**, *11*, 2202933.
[4] L. E. MacKenzie, R. Pal, *Nat. Rev. Chem.* **2020**, *5*, 109.
[5] F. Zinna, L. Arrico, T. Funaioli, L. Di Bari, M. Pasini, C. Botta, U. Giovanella, *J. Mater. Chem. C* **2022**, *10*, 463.
[6] A. G. Dumanli, T. Savin, *Chem. Soc. Rev.* **2016**, *45*, 6698.
[7] L. Wan, R. Zhang, E. Cho, H. Li, V. Coropceanu, J.-L. Brédas, F. Gao, *Nat. Photonics* **2023**, *17*, 649.
[8] F. Furlan, J. M. Moreno-Naranjo, N. Gasparini, S. Feldmann, J. Wade, M. J. Fuchter, *Nat. Photonics* **2024**, *18*, 658.
[9] J. M. Moreno-Naranjo, F. Furlan, J. Wang, S. T. J. Ryan, T. Matulaitis, Z. Xu, Q. Zhang, L. Minion, M. D. Girolamo, T. Jávorfi, G. Siligardi, J. Wade, N. Gasparini, E. Zysman-Colman, M. J. Fuchter, *Adv. Mater.* **2024**, *36*, 2402194.
[10] J. Wade, F. Salerno, R. C. Kilbride, D. K. Kim, J. A. Schmidt, J. A. Smith, L. M. LeBlanc, E. H. Wolpert, A. A. Adeleke, E. R. Johnson, J. Nelson, T. Mori, K. E. Jelfs, S. Heutz, M. J. Fuchter, *Nat. Chem.* **2022**, *14*, 1383.
[11] G. Albano, G. Pescitelli, L. Di Bari, *Chem. Rev.* **2020**, *120*, 10145.
[12] S. M. Morrow, A. J. Bissette, S. P. Fletcher, *Nat. Nanotechnol.* **2017**, *12*, 410.
[13] G. Lakhwani, S. C. J. Meskers, *J. Phys. Chem. A* **2012**, *116*, 1121.
[14] S. C. J. Meskers, *Mater. Adv.* **2022**, *3*, 2324.
[15] Z. Gong, T. Dan, J. Chen, Z. Li, J. Yao, Y. Zhong, *Angew. Chem., Int. Ed.* **2024**, *63*, 202402882.
[16] F. Zinna, U. Giovanella, L. Di Bari, *Adv. Mater.* **2015**, *27*, 1791.
[17] F. Zinna, G. Pescitelli, L. Di Bari, *Chirality* **2020**, *32*, 765.
[18] F. Zinna, M. Pasini, F. Galeotti, C. Botta, L. Di Bari, U. Giovanella, *Adv. Funct. Mater.* **2017**, *27*, 1603719.
[19] L. Wan, Y. Liu, M. J. Fuchter, B. Yan, *Nat. Photonics* **2023**, *17*, 193.
[20] E. Plum, N. I. Zheludev, *Appl. Phys. Lett.* **2015**, *106*, 221901.
[21] T.-L. Chen, A. Salij, K. A. Parrish, J. K. Rasch, F. Zinna, P. J. Brown, G. Pescitelli, F. Urraci, L. A. Aronica, A. Dhavamani, M. S. Arnold, M. R. Wasielewski, L. Di Bari, R. Tempelaar, R. H. Goldsmith, *Nat. Commun.* **2024**, *15*, 3072.
[22] A. H. Salij, R. H. Goldsmith, R. Tempelaar, *Nat. Commun.* **2024**, *15*, 340.
[23] X. Hou, F. Li, Y. Song, M. Li, *J. Phys. Chem. Lett.* **2022**, *13*, 2885.
[24] M. Zhang, Y. Wang, Y. Zhou, H. Yuan, Q. Guo, T. Zhuang, *Nanoscale* **2022**, *14*, 592.
[25] X. Zhang, Y. Xu, C. Valenzuela, X. Zhang, L. Wang, W. Feng, Q. Li, *Light: Sci. Appl.* **2022**, *11*, 223.
[26] O. Arteaga, *Thin Solid Films* **2016**, *617*, 14.
[27] G. Picard, D. Simon, Y. Kadiri, J. D. LeBreux, F. Ghozayel, *Langmuir* **2012**, *28*, 14799.
[28] C. Xu, C. Huang, H. Huang, *Appl. Mater. Today* **2021**, *22*, 100912.
[29] Md. J. Abedin, P. V. D. Schoot, G. Garnier, M. Majumder, *Langmuir* **2023**, *39*, 6142.
[30] Technical Association of Pulp and Paper Industry (TAPPI) in TAPPI Standards: Regulations and Style Guidelines, Standard Terms and Their Definition for Cellulose Nanomaterials, ISO/TS20477, **2017**.
[31] A. Operamolla, *Int. J. Photoenergy* **2019**, *2019*, 3057929.
[32] A. Operamolla, C. Mazzuca, L. Capodieci, F. Di Benedetto, L. Severini, M. Titubante, A. Martinelli, V. Castelvetro, L. Micheli, *ACS Appl. Mater. Interfaces* **2021**, *13*, 44972.
[33] L. Spagnuolo, R. D'Orsi, A. Operamolla, *ChemPlusChem* **2022**, *87*, 202200204.
[34] X.-R. Ong, A. X. Chen, N. Li, Y. Y. Yang, H.-K. Luo, *Small Sci.* **2023**, *3*, 2200076.
[35] B. Thomas, M. C. Raj, K. B. Athira, M. H. Rubiya, J. Joy, A. Moores, G. L. Drisko, C. Sanchez, *Chem. Rev.* **2018**, *118*, 11575.
[36] N. Lin, A. Dufresne, *Nanoscale* **2014**, *6*, 5384.
[37] R. H. Marchessault, F. F. Morehead, N. M. Walter, *Nature* **1959**, *184*, 632.
[38] M. J. Friedel, *Ann. Phys.* **1922**, *18*, 273.
[39] G. F. Dionne, G. A. Allen, P. R. Haddad, C. A. Ross, B. Lax, *Lincoln Lab. J.* **2005**, *15*, 323.
[40] R. M. Parker, B. Frka-Petesic, G. Guidetti, G. Kamita, G. Consani, C. Abell, S. Vignolini, *ACS Nano* **2016**, *10*, 8443.
[41] R. M. Parker, G. Guidetti, C. A. Williams, T. Zhao, A. Narkevicius, S. Vignolini, B. Frka-Petesic, *Adv. Mater.* **2018**, *30*, 1704477.
[42] J. R. Bruckner, A. Kuhnhold, C. Honorato-Rios, T. Schilling, J. P. F. Lagerwall, *Langmuir* **2016**, *32*, 9854.
[43] M. Xu, W. Li, C. Ma, H. Yu, Y. Wu, Y. Wang, Z. Chen, J. Li, S. Liu, *J. Mater. Chem. C* **2018**, *6*, 5391.
[44] X. M. Dong, D. G. Gray, *Langmuir* **1997**, *13*, 2404.
[45] W. J. Orts, L. Godbout, R. H. Marchessault, J.-F. Revol, *Macromolecules* **1998**, *31*, 5717.
[46] Y. Huang, Y. Qian, Y. Chang, J. Yu, Q. Li, M. Tang, X. Yang, Z. Liu, H. Li, Z. Zhu, W. Li, F. Zhang, G. Qing, *Adv. Mater.* **2024**, *36*, 2308742.
[47] H. Zheng, W. Li, W. Li, X. Wang, Z. Tang, S. X. Zhang, Y. Xu, *Adv. Mater.* **2018**, *30*, 1705948.
[48] J. Tao, C. Zou, H. Jiang, M. Li, D. Lu, S. Mann, Y. Xu, *CCS Chem.* **2021**, *3*, 932.
[49] H. Zheng, B. Ju, X. Wang, W. Wang, M. Li, Z. Tang, S. X. Zhang, Y. Xu, *Adv. Opt. Mater.* **2018**, *6*, 1801246.
[50] Z. Wang, J. Chu, L. Shi, T. Xing, X. Gao, Y. Xu, *Small* **2024**, *20*, 2306810.
[51] D. Qu, M. Archimi, A. Camposeo, D. Pisignano, E. Zussman, *ACS Nano* **2021**, *15*, 8753.
[52] D. Lu, X. Yu, S. Zhu, Y. Xu, *Cellulose* **2023**, *30*, 8325.
[53] D. Lu, M. Li, X. Gao, X. Yu, L. Wei, S. Zhu, Y. Xu, *ACS Nano* **2023**, *17*, 461.
[54] *Comprehensive Chiroptical Spectroscopy: Instrumentation, Methodologies, and Theoretical Simulations* (Eds.:N. Berova, P. L. Polavarapu, K. Nakanishi, R. W. Woody) Wiley, Hoboken, New Jersey **2011**.
[55] E. M. Sánchez-Carnerero, A. R. Agarrabeitia, F. Moreno, B. L. Maroto, G. Muller, M. J. Ortiz, S. de la Moya, *Chem.-Eur. J.* **2015**, *21*, 13488.
[56] L. Arrico, L. Di Bari, F. Zinna, *Chem.-Eur. J.* **2021**, *27*, 2920.
[57] L. Llanos, P. Cancino, P. Mella, P. Fuentealba, D. Aravena, *Coord. Chem. Rev.* **2024**, *505*, 215675.
[58] D. F. Caffrey, T. Gorai, B. Rawson, M. Martínez-Calvo, J. A. Kitchen, N. S. Murray, O. Kotova, S. Comby, R. D. Peacock, P. Stachelek, R. Pal, T. Gunnlaugsson, *Adv. Sci.* **2024**, *11*, 2307448.
[59] I. M. S. Diogenis, A. G. Bispo-Jr, R. V. Pirovani, L. F. Saraiva, F. C. Gozzo, C. R. D. Correia, I. O. Mazali, R. A. Nome, F. A. Sigoli, *J. Mater. Chem. C* **2024**, *12*, 5097.
[60] O. G. Willis, F. Zinna, L. Di Bari, *Angew. Chem., Int. Ed.* **2023**, *62*, 202302358.
[61] H.-Y. Wong, W.-S. Lo, K.-H. Yim, G.-L. Law, *Chem* **2019**, *5*, 3058.
[62] Y. Kitagawa, S. Wada, M. D. J. Islam, K. Saita, M. Gon, K. Fushimi, K. Tanaka, S. Maeda, Y. Hasegawa, *Commun. Chem.* **2020**, *3*, 119.
[63] B.-A. N. Willis, D. Schnable, N. D. Schley, G. Ung, *J. Am. Chem. Soc.* **2022**, *144*, 22421.
[64] M. Deng, N. D. Schley, G. Ung, *Chem. Commun.* **2020**, *56*, 14813.
[65] F. Zinna, L. Di Bari, *Chirality* **2015**, *27*, 1.
[66] X. Wang, Q. Miao, W. Zhang, Y. Zhou, R. Xiong, Y. Duan, X. Meng, C. Ye, *Chem. Eng. J.* **2024**, *481*, 148463.
[67] M. Xu, Z. Xu, M. A. Soto, Y. Xu, W. Y. Hamad, M. J. MacLachlan, *Adv. Mater.* **2023**, *35*, 2301060.
[68] Y. Shi, Z. Zhou, X. Miao, Y. J. Liu, Q. Fan, K. Wang, D. Luo, X. W. Sun, *J. Mater. Chem. C* **2020**, *8*, 1048.

[69] L. Xing, G. Li, Y. Sun, X. Wang, Z. Yuan, Y. Fu, M. Qin, *Carbohydr. Polym.* **2023**, *313*, 120856.
[70] J. He, K. Bian, N. Li, G. Piao, *J. Mater. Chem. C* **2019**, *7*, 9278.
[71] R. Wang, P. Yu, J. Tan, Y. Zhou, J. Zhang, *Polyoxometalates* **2022**, *1*, 9140009.
[72] L. K. Bast, K. W. Klockars, L. G. Greca, O. J. Rojas, B. L. Tardy, N. Bruns, *Biomacromolecules* **2021**, *22*, 2067.
[73] M. Górecki, L. Carpita, L. Arrico, F. Zinna, L. Di Bari, *Dalton Trans.* **2018**, *47*, 7166.
[74] M. Tsurui, R. Takizawa, Y. Kitagawa, M. Wang, M. Kobayashi, T. Taketsugu, Y. Hasegawa, *Angew. Chem., Int. Ed.* **2024**, *63*, 202405584.
[75] J. Kumar, B. Marydasan, T. Nakashima, T. Kawai, J. Yuasa, *Chem. Commun.* **2016**, *52*, 9885.
[76] J. L. Lunkley, D. Shirotani, K. Yamanari, S. Kaizaki, G. Muller, *J. Am. Chem. Soc.* **2008**, *130*, 13814.
[77] J. L. Lunkley, D. Shirotani, K. Yamanari, S. Kaizaki, G. Muller, *Inorg. Chem.* **2011**, *50*, 12724.